The atmospheric settling of commercially sold microplastics

Alina Sylvia Waltraud Reininger[1], Daria Tatsii[1], Taraprasad Bhowmick[2], Gholamhossein Bagheri[2], and Andreas Stohl[1]

[1]Department of Meteorology and Geophysics, University of Vienna, Josef-Holaubek-Platz 2, 1090 Vienna, Austria
[2]Laboratory for Fluid Physics, Pattern Formation and Biocomplexity, Max Planck Institute for Dynamics and Self-Organization, Am Fassberg 17, 37077 Göttingen, Germany

Correspondence: Alina Sylvia Waltraud Reininger (alina.reininger@univie.ac.at)

Abstract. The atmosphere plays a major role in the dispersion of microplastics in the environment. The atmospheric transport of large microplastics is strongly influenced by their settling behavior, which depends on their physical properties, including size and shape. However, experimental data on the settling behavior of commercially available microplastics with complex, nonspherical shapes in air are rare. Here we present experiments on the gravitational settling velocity of commercially available

5 glitters (nominal diameters between 0.1 and 3 mm) and fibers (lengths between 1.2 and 5 mm). We observed that glitters and fibers settle up to 74 % and 78 % slower compared to volume-equivalent spheres, respectively. The atmospheric transport of fibers has been studied previously; however, there are no studies on the atmospheric transport potential of glitters. Therefore, we used an atmospheric transport model constrained by our experimental results to assess the transport potential of glitters. Our results reveal that glitters exhibit transport distances 12–261 % greater than volume-equivalent spheres, highlighting their

10 elevated atmospheric transport potential. As a result, the environmental impact of glitter particles, especially following their use in entertainment events, warrants attention and mitigation.

1 Introduction

Microplastics, synthetic polymers ranging from 1 to 5000 μm in size, are a major source of pollution worldwide (Petersen and Hubbart, 2021). They can be categorized as either primary microplastics - manufactured intentionally for products such

15 as cosmetics, cleaning agents, and personal care products (Auta et al., 2017) - or secondary microplastics, formed by the fragmentation of larger plastics (Petersen and Hubbart, 2021). Shapes of microplastics include films, irregular particles, fibers, spheres, and spheroids (Hartmann et al., 2019), with the observed shapes often differing by location (Zhang et al., 2020; Petersen and Hubbart, 2021). In many studies of urban locations, for example, fibers have been identified as the most common shape of microplastics (Dris et al., 2015; Liu et al., 2019a; Zhou et al., 2017; Cai et al., 2017). Fibers are also the dominant

20 shape observed in several remote locations (Brahney et al., 2020; Cabrera et al., 2020; Ambrosini et al., 2019). Similar to fibers, films have been detected in both urban (Abbasi et al., 2019; Cai et al., 2017; Zhou et al., 2017) and remote locations (Allen et al., 2020; Cabrera et al., 2020). Glitter - small, flat, reflective particles ranging from 50 μm up to 6350 mm, with 200 μm being the most popular size (Yurtsever, 2019b; Blackledge and Jones Jr., 2007) - is classified as a primary microplastic. Glitter particles can be described as films or irregular particles according to the nomenclature recommendations of Hartmann

25 et al. (2019), or disks, as done by Tinklenberg et al. (2023, 2024). The production typically involves plastics, metal foils, or dyes (Tagg and Ivar do Sul, 2019; Zanini et al., 2024). As an alternative, renewable, plant-based raw material, such as seaweed, regenerated cellulose, mica powders, and glycerin are produced (Yurtsever, 2019b; Zanini et al., 2024). According to the report of Market Research Intellect (2025), the glitter powder market was valued at USD 100 Million in 2023 and is expected to reach USD 324.34 Million by 2031. The growth in glitter powder industry can be attributed to its broad application and an

30 increasing demand in many sectors, such as the automobile, textile, and cosmetic industries (Market Research Intellect, 2025; Zanini et al., 2024). Furthermore, there is a growing interest in crafting activities where glitter powder is added to decorations, gift cards, and arts (Market Research Intellect, 2025; Yurtsever, 2019a). Glitter is also extensively used in the entertainment sector for decorations, stage sets, special effects, and events such as carnivals and shows (Yurtsever, 2019a; Zanini et al., 2024; Market Research Intellect, 2025).

35 Microplastics are associated with substantial harmful effects on the environment. Several studies have investigated the adverse effects (e.g., acute toxicity, increased susceptibility to pollutants and mortality, reduced food intake, and potential bioaccumulation) of microplastic fibers on soil and aquatic organisms (Gray and Weinstein, 2017; Romanó de Orte et al., 2019; Kwak et al., 2022; Song et al., 2019; Kim et al., 2021). Furthermore, airborne fibers have the potential to harm the human respiratory systems (Prata, 2018). However, glitter has received less scientific attention than fibers (Yurtsever, 2019b; Zanini

40 et al., 2024). Glitter has been reported in riverbed and coastal sediments, surface waters (Nithin et al., 2022; Ballent et al., 2016), wastewater treatment plants (Lusher et al., 2017; Raju et al., 2020), and street dust (Abbasi et al., 2017, 2019; Dehghani et al., 2017). Due to the recycling of biosolids, glitter poses a threat to farm soil and soil invertebrates (Harley-Nyang et al., 2022; Dąbrowska, 2022; Medyńska-Juraszek and Jadhav, 2022; Chen et al., 2024). Both conventional and biodegradable glitter cause ecological impacts in aquatic ecosystems (Green et al., 2021; Luana Lume Yoshida and da Cunha-Santino, 2023). In

45 aquatic organisms, glitter is associated with internal damage, adverse effects on embryonic development, biovolume increment, an increase in antioxidant defense, and reducing survival, feeding, hatch, and growth rates (Abessa et al., 2023; Machado et al., 2023; Provenza et al., 2022; Das Pramanik et al., 2023).

For transporting microplastics to different environmental media, the atmosphere plays an important role (Allen et al., 2020; Bergmann et al., 2019; Dris et al., 2016; Liu et al., 2019b). Particle shape is a key factor influencing the atmospheric transport

50 potential of microplastics, primarily through its effect on terminal settling velocity v_t. A particle obtains its terminal settling velocity when the force of gravity is balanced by the drag force. v_t is calculated by:

$$v_t = \left[\frac{4}{3} C_{cun} g \frac{d_{eq}}{C_D} \frac{\rho_p}{\rho_a} \right]^{1/2}, \tag{1}$$

where g is the gravitational acceleration, C_{cun} is the Cunningham slip correction factor (which accounts for reduced drag on particles < 1 μm), d_{eq} is the volume-equivalent diameter of a sphere, ρ_p and ρ_a are the densities of the particle and the air,

55 respectively, and C_D is the dimensionless drag coefficient, which depends on the particle's shape and orientation (Bagheri and Bonadonna, 2016).

Only a limited number of experimental studies have examined the settling behavior of microplastic films, disks, and fibers in air (Qi et al., 2012; Preston et al., 2023; Tatsii et al., 2024; Tinklenberg et al., 2023, 2024). This study is the first to

investigate the atmospheric transport potential of glitter in the size range of 50 µm to 3 mm. For that, we conducted laboratory
experiments to measure the gravitational settling behavior of microplastic glitters of six sizes. Additionally, we examined the
settling behavior of eight sizes of commercially available microplastic fibers with lengths ranging from 1.2 to 5 mm. Such
fibers, in contrast to the 3D-printed fibers used by Tatsii et al. (2024), can contain imperfections that might impact their settling
behavior. These experimental findings were then integrated into an atmospheric transport model to evaluate the residence times
and travel distances of glitter particles, as the atmospheric transport potential of fibers has been investigated in detail by Tatsii
et al. (2024).

2 Methods

2.1 Particle properties

Experiments were performed for six different sizes of glitter particles (craft glitter, Hemway), characterized by hexagonal or
irregular shapes. These glitter particles have nominal diameters of 0.1, 0.2, 0.4, 0.6, 1, and 3 mm, with longest dimensions
L from 0.18 - 3.29 mm (Table 1). Their densities were determined with a helium pycnometer (AccuPyc II 1340 V3.00,
Micromeritics Instrument Corporation), resulting in an average density of 1.39 g/cm^3, ranging from 1.38 - 1.40 g/cm^3. The
glitter particles' dimensions were determined using a 3D laser microscope (VK-X260K, KEYENCE International (Belgium)
NV/SA) and the software ImageJ. The sphericity Ψ, which compares the surface area of a sphere to that of a nonspherical
particle with equivalent volume, ranges from 0.83 to 0.19. It is defined as $\Psi = \pi d_{eq}^2/SA$, with SA being the surface area of
the particle.

The fibers consist of Polyamide 6.6 Precision Cut Flock (Flockan) with a density of 1.15 g/cm^3. Eight fiber sizes were
studied, with lengths ranging from 1.2 to 5 mm and diameters between 10 and 105 µm (Table 2). The fibers possess aspect
ratios AR (longest dimension L / shortest dimension S) between 36 and 121 and no or a small curvature. The sphericity ranges
from 0.11 to 0.01. Microscopic images of the glitter particles and fibers are presented in Fig. 1(a)-(d) and Fig. S1-S3.

2.2 Experimental setup

In our experimental setup, one can measure the three-dimensional translational and rotational motion of solid particles between
0.1 - 5 mm in quiescent air. Details of the setup, as well as the postprocessing and calibration processes, are described in
Bhowmick et al. (2024a) and Tatsii et al. (2024). This setup consists of an air-filled chamber ($90 \times 90 \times 200$ mm) where the
particles can settle under gravity. Four high-speed cameras (Phantom VEO4K 990L, Vision Research) synchronized with a
high-intensity pulsed white LED array (LED-Flashlight 300, LaVision GmbH) surround the chamber. Particles are introduced
into the chamber using an injector mounted on a detachable top cover. Notice that insertion speeds are chosen to be close to
expected terminal settling velocities, so particles can accelerate or decelerate in the air column, depending on whether insertion
is slower or faster than the terminal settling velocity. For the experiments, the resolution of the cameras was set to 4096×1140
pixels, each pixel corresponding to a physical area of 6.75×6.75 µm^2. The exposure time was set to 5 µs. For samples 1-4 of

90 the fibers, a frame rate of 200 frames per second was chosen. For all other particles, the frame rate was set to 1492 frames per second.

Prior to the experiments, the model of Bagheri and Bonadonna (2016, 2019) was used to estimate the vertical distance at which the particles approximately reach their terminal velocity. The settling chamber was positioned accordingly to allow the cameras to capture particles near their steady-state velocity. After calibration, the particles were individually released into the

95 settling chamber. When a particle was observed by all four cameras, the images were stored for postprocessing. Figure 1(e)-(h) and Fig. S4-S5 illustrate overlays of particle images recorded by the cameras.

2.3 Postprocessing and data analysis

Following the method outlined in Bhowmick et al. (2024a), for each camera, a median image background was calculated using all available frames and subsequently subtracted from the images. Then, a small region around the particle was cropped, and the

100 resulting image was independently thresholded. The centroid position and longest length were extracted from the thresholded image using the OpenCV 2 library in Python. The centroids were used to determine the three-dimensional positions of the particles, and the velocities were extracted using a sixth-order finite difference scheme.

To ensure that the terminal settling velocity had been reached, only experimental runs with relative changes in velocity of less than 10 % over a wide number of frames were chosen. Figure 1(i)-(l) shows the postprocessed settling velocities corresponding

105 to the particles shown in Fig. 1(a)-(d). Noise that was caused by an inaccurate estimation of the centroid position was removed by applying a Savitzky-Golay filter. For the selected experimental runs, the settling velocities were averaged over the number of frames. Then the settling velocities obtained for individual particles were averaged over the number of experiments performed for each particle type.

2.4 Drag coefficient of nonspherical particles

110 For describing the drag coefficient of spheres, accurate analytical and empirical models exist (Clift and Gauvin, 1971). For nonspherical particles, such generalized models do not exist; however, some empirical relationships have been determined as a function of particle shape. According to Coyle et al. (2023) and Saxby et al. (2018), the semi-empirical settling scheme of Bagheri and Bonadonna (2016) provides excellent results for the drag coefficient of nonspherical particles of various shapes. This scheme is suited for regular and irregular particle shapes and Reynolds numbers smaller than $3 \cdot 10^5$. Bagheri and

115 Bonadonna (2016)'s scheme considers the particle's flatness ($f = S/I$) and elongation ($e = I/L$), where L, I, and S are the particle's longest, intermediate, and shortest dimensions, respectively. The model distinguishes between random-orientation-drag (i.e., drag coefficient C_D of the particle when averaged over many random orientations), maximum-orientation-drag (i.e., C_D when the particle's maximum projection area is normal to gravity), and also minimum-orientation-drag (i.e., C_D when the particle's minimum projection area is normal to gravity). Additionally, an average between the predictions for

120 random-orientation-drag and maximum-orientation-drag has been introduced by Tatsii et al. (2024), hereafter referred to as the average-orientation-drag model. Equations S1-S11 describe the chain of equations to calculate the drag coefficient as a function of various shape descriptors introduced by Bagheri and Bonadonna (2016). There is also a simplified version of the
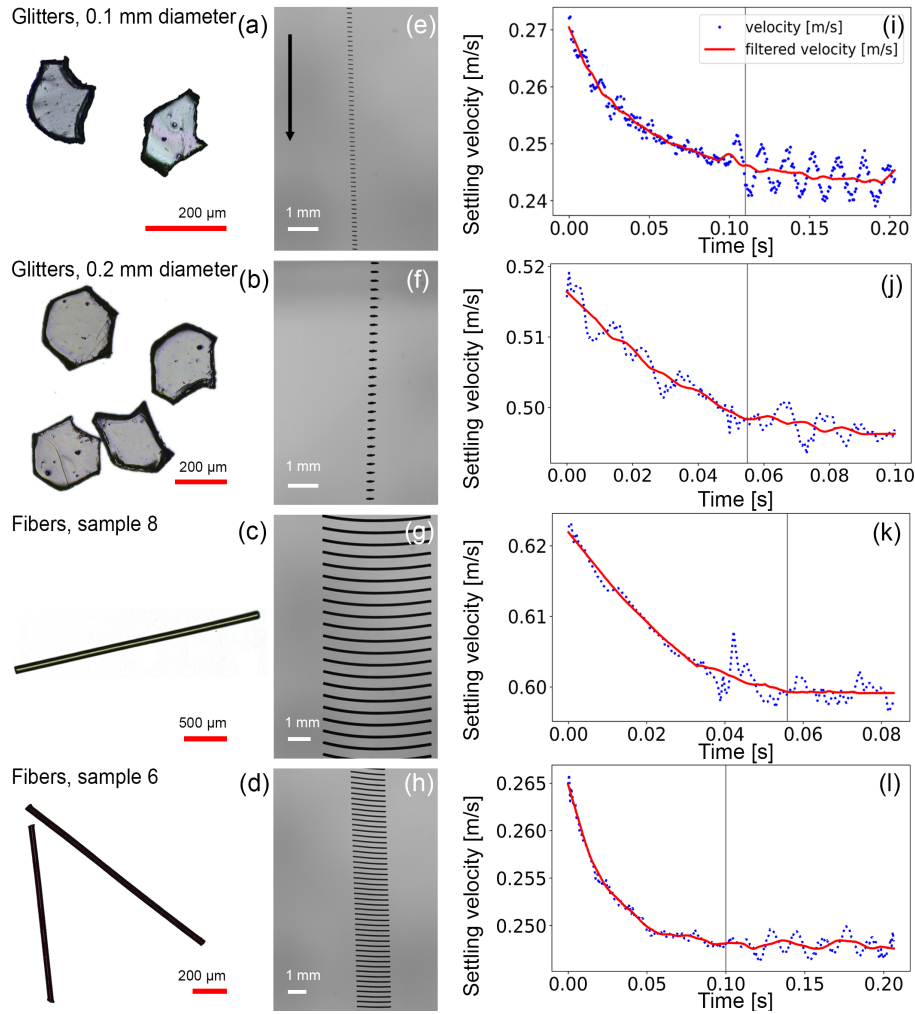
Figure 1. Example of the glitters and fibers and their settling behavior. (a)-(d): Microscopic images of glitter particles and fibers. (e)-(h): Overlays of particle images recorded by the cameras. The vertical vector shows the direction of gravity. (i)-(l): The postprocessed velocity time series of the particles. The dots represent the experimental postprocessed data, and the filtered data are shown as solid red lines. The right half of the dashed grey line in panels (i)-(l) indicates the data selected for the settling velocity analysis.

model in which the shape of the particle is approximated by an ellipsoid of similar form by neglecting the term $\frac{d_{eq}^3}{L\,I\,S}$ in the Stokes' form factor F_S and in Newton's form factor F_N (Bagheri and Bonadonna, 2016, 2019). In this study, the full model version is used for both glitters and fibers, however, we also provide results using the simplified model for fibers, as suggested by Tatsii et al. (2024). The settling velocities of the volume-equivalent spheres are not measured but modeled with the full model version, since the settling velocities of spheres are well known and need no further investigation.

125

2.5 Atmospheric transport modeling

We simulated the atmospheric transport of the glitter sizes used in the experiments, and also for the smallest commercially available glitter particles (0.05 mm nominal diameter; no experiments performed) using the Lagrangian transport and dispersion model FLEXPART version 11 (Bakels et al., 2024). The atmospheric transport of fibers has been investigated in detail before, for example by Tatsii et al. (2024). FLEXPART simulates the transport, turbulent diffusion, dry and wet deposition, decay, and first-order chemical reactions of tracers from local to global scales released from point, line, area, or volume sources (Pisso et al., 2019). The full, maximum-orientation-drag model of Bagheri and Bonadonna (2016) was used for calculating settling velocities for the simulations. The simulations were conducted for the year 2020 by releasing 10 000 glitter particles and their respective volume-equivalent spheres at altitudes 10 - 100 m above ground level. Releases occurred at 03:00 and 15:00 local time on the 1st and 15th of each month in six cities, representing a range of meteorological conditions controlling wet and dry deposition: London (51°30'N 0°7'W), Shanghai (31°13'N 121°28'E), Brasília (15°47'S 47°52'W), Cairo (30°1'N 31°14'W), New Orleans (29°57'N 90°4' W), and Reykjavík (64°7'N 21°49'W). As input for the simulations, ECMWF ERA5 global meteorological fields at 0.5 ° x 0.5 ° horizontal and 1-hour temporal resolution were used (Hersbach et al., 2020). The output was produced with 0.5 ° x 0.5 ° horizontal resolution and concentrations are sample from 6 seconds to 900 s, depending on particle size. Around the release points, nested grids were used with resolutions of 0.005, 0.0005, and 0.0001 ° for glitters and spheres with nominal diameters of 0.05 mm, 0.1 mm, and 0.2 - 3 mm, respectively. Based on the simulations' output, average atmospheric residence times and transport distances of the particles were determined. The mean atmospheric transport distance is calculated from the distance of grid cell ij from the release point, D_{ij} and the total mass deposited in grid cell ij, M_{ij}:

$$\bar{D} = \frac{\sum_{ij} D_{ij} \cdot M_{ij}}{\sum_{ij} M_{ij}} \tag{2}$$

The relative decrease in total atmospheric particle mass as a function of time t was averaged over the number of releases and fitted to $y = e^{-\frac{t}{t_e}}$. Residence times were then determined as e-folding times t_e.

3 Results and discussion

3.1 Gravitational settling of glitters

The measured gravitational settling velocities for glitter particles range from 0.221 m s^{-1} to 1.139 m s^{-1}, whereas the corresponding calculated settling velocities of volume-equivalent spheres range from 0.393 m s^{-1} to 4.373 m s^{-1} (Fig. 2a). The gravitational settling velocities of glitters are reduced by 42 % to 74 % compared to volume-equivalent spheres (Table 1). The relative differences between the settling velocities of spherical and nonspherical particles tend to increase with increasing particle size and decreasing sphericity Ψ. The greatest reductions in settling velocity occur for glitters with the largest aspect ratios ($L/S \geq 22$), where settling velocities are only 43 and 26 % of those of volume-equivalent spheres.

Figure 2(c) compares the observed gravitational settling velocities of the glitters with those predicted by the model of Bagheri and Bonadonna (2016, 2019), shown in Table 1. With average-orientation-drag configuration, the model of Bagheri

and Bonadonna (2016, 2019) agrees well with the measurements, with a relative difference of 14.4 %. The highest deviations are received with random-orientation-drag configuration (19.0 %). This configuration performs well for large glitter particles (nominal diameters > 0.4 mm), with a relative difference of 3.6 %, but performs less accurately for smaller particles (0.1 and 0.2 mm nominal diameters), with an average relative difference of 26.3 %. The best overall agreement is achieved for maximum-orientation-drag configuration, which yields an average relative difference of 13.2 %. This configuration shows the most accurate predictions for particles $\leq$ 0.2 mm, with an average relative difference of 5.2 %. In general, the model of Bagheri and Bonadonna (2016, 2019) overestimates the settling velocities of small glitters and underestimates those of large glitters. It should also be noted that the estimation of settling velocities is based on the mean of the measured dimensions and the nominal shapes of the particles given by the manufacturer, which may be subject to some variation, as shown in Fig. 1 and Fig. S1-S3. As a result, the discrepancies between the model of Bagheri and Bonadonna (2016, 2019) and the glitter particles are partly attributable to imperfections in the shape and size of the particles.

Overall, as particle size increases, the comparison of observed and modeled settling velocities suggests a shift from maximum-orientation-drag to average-orientation-drag, and then to random-orientation-drag aligning most closely. This can best be seen in Fig. 2(c), which compares modeled and observed settling velocities. In fact, in our experiments we observed that the smallest glitters (0.1 and 0.2 mm nominal diameters) reached a terminal, steady-state orientation with their largest projection area perpendicular to the settling direction. In contrast, for larger glitter particles, tumbling motions occurred that increased with increasing particle size. This is in agreement with the observed shift of the best-suited particle-orientation model with particle size. In literature, a Reynolds number $Re \approx 100$ is quoted as a threshold below which particles tend to fall with their maximum projection area normal to the direction of gravity (Bagheri and Bonadonna, 2016; Willmarth et al., 1964). However, in our experiments, tumbling motions occur already at $Re < 100$, from about $Re = 17$ and becoming quite pronounced at $Re = 69$. Further investigation is needed to ascertain whether this discrepancy arises from differences in particle shapes or from variations in the experimental setups, each with its distinct capabilities and limitations.
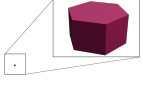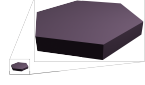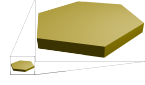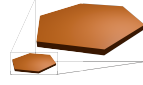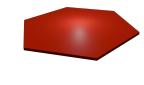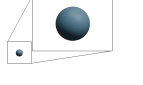
3.2 Gravitational settling of fibers

The measured gravitational settling velocities for fibers range from 0.033 m s^{-1} to 0.618 m s^{-1}, whereas the corresponding calculated settling velocities of volume-equivalent spheres range from 0.102 m s^{-1} to 1.926 m s^{-1} (Fig. 2b). The settling velocities of fibers are reduced by 58 - 78 % compared to volume-equivalent spheres (Table 2). As with the glitters, the largest differences are observed for fibers with the largest aspect ratios ($L/S = 63, 121$).

Figure 2(d) presents a comparison of the modeled and experimental settling velocities of the fibers. The scheme of Bagheri and Bonadonna (2016, 2019) agrees best with the experiments with maximum-orientation-drag configuration, with a deviation of 12.4 %. For average-orientation-drag, the relative difference is 21.6 % and the largest deviation occurs again with random-orientation-drag (31.7 %).

In our experiments, most fibers achieved a terminal, steady-state orientation with their largest projected area normal to gravity, which is in agreement with previous work (Tatsii et al., 2024; Bhowmick et al., 2024a, b; Newsom and Bruce, 1994). This explains why the maximum-orientation-drag configuration works best for all particle sizes. The simplified average-orientation-

Table 1. Characteristics of the Glitters and Their Modeled and Measured Settling Velocities[a]
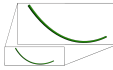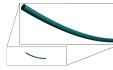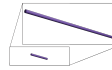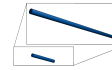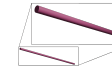
Nominal diameter	0.05 mm	0.1 mm	0.2 mm	0.4 mm	0.6 mm	1 mm	3 mm
Symbol							
d_{eq} (µm)	42.6	110.8	187.5	261.7	316.4	478.9	929.0
L (µm)	50.0	175.8	305.9	496.5	672.2	1240.7	3287.1
I (µm)	43.3	132.3	247.5	405.4	538.9	996.4	2683.1
S (µm)	25.0	26.7	56.8	58.6	56.5	57.5	59.8
L/S	2	7	5	8	12	22	55
fl	0.58	0.20	0.23	0.14	0.10	0.06	0.02
el	0.87	0.75	0.81	0.82	0.80	0.78	0.82
Ψ	0.83	0.71	0.64	0.53	0.45	0.31	0.19
Re	0.18	1.60	5.91	11.85	17.41	32.60	69.19
N	-	11	5	3	3	2	3
$v_{\rm t}$ (m/s)	-	0.221	0.483	0.664	0.842	1.041	1.139
σ_{vt} (m/s)	-	0.014	0.047	0.005	0.019	1.135	0.062
$v_{\max}$ (m/s)	0.067	0.243	0.488	0.608	0.654	0.779	0.927
$v_{\rm aver}$ (m/s)	0.069	0.270	0.548	0.688	0.741	0.876	1.005
$v_{\rm rand}$ (m/s)	0.072	0.308	0.637	0.812	0.875	1.019	1.107
Symbol							
$v_{\rm sph}$ (m/s)	0.073	0.393	0.837	1.271	1.564	2.404	4.373
$v_{\rm t}/v_{\rm sph}$	-	0.56	0.58	0.52	0.54	0.43	0.26

[a] $d_{\rm eq}$ is the volume equivalent diameter of a sphere, L is the longest, I the intermediate, and S the shortest dimension of the particle. fl is the particle's flatness and el is its elongation. Ψ is the sphericity, which compares the surface area of a particle to that of sphere $\pi d_{eq}^2/SA$, with SA being the surface area of the particle. The Reynolds number Re is defined as $\rho_a v_{\rm t} d_{eq}/\nu$, where ρ_a is the density and ν is the kinematic viscosity of the air. N is the number of successful experiments. The measured settling velocity $v_{\rm t}$ is given as the average over the number of experiments of the corresponding shape and size, with σ_{vt} being the standard deviation. $v_{\rm rand}$, $v_{\max}$, $v_{\rm aver}$, and $v_{\rm sph}$ are the modeled velocities with random-, maximum-, and average-orientation-drag, and for volume equivalent spheres, respectively. For glitters with nominal diameters of 0.05 mm, no experiments but simulations have been performed, and their properties are listed for completeness sake.

drag model works well for fibers too (Table S1), similar to the study of Tatsii et al. (2024). For the simplified model, the best agreement is again achieved for maximum-orientation-drag configuration, with a relative difference of 7.3 %, followed by average-orientation-drag configuration (13.2 %). The largest difference occurs for random-orientation drag (24.3 %). However, Tatsii et al. (2024) investigated custom-produced fibers with sub-micron precision, minimizing the occurrence of imperfection and irregularities. In contrast, the commercially available fibers examined here are associated with certain deviations from the nominal size and shape, which introduces some uncertainties in the comparisons.

Table 2. Characteristics of the Fibers and Their Modeled and Measured Settling Velocities[b]

Name	Sample 1	Sample 2	Sample 3	Sample 4	Sample 5	Sample 6	Sample 7	Sample 8
Symbol								
d_{eq}(μm)	56.5	107.6	108.4	117.9	175.5	193.1	280.4	435.7
L(μm)	1200	2300	1500	1500	1500	2000	3000	5000
$I = S$(μm)	10	19	24	27	49	49	70	105
L/S	120	121	63	56	31	41	43	48
fl	1	1	1	1	1	1	1	1
el	0.01	0.01	0.07	0.02	0.03	0.02	0.02	0.02
Ψ	0.11	0.06	0.05	0.05	0.03	0.03	0.02	0.01
Re	0.11	0.49	0.50	0.85	2.87	3.16	6.97	17.66
N	2	8	11	8	13	10	8	7
v_t (m/s)	0.033	0.071	0.073	0.112	0.246	0.248	0.382	0.618
σ_{vt} (m/s)	0.004	0.003	0.006	0.007	0.017	0.015	0.020	0.081
v_{max} (m/s)	0.024	0.076	0.098	0.118	0.264	0.275	0.439	0.702
v_{aver} (m/s)	0.026	0.085	0.110	0.132	0.298	0.311	0.498	0.800
v_{rand} (m/s)	0.030	0.097	0.125	0.151	0.347	0.362	0.587	0.952
Symbol								
v_{sph} (m/s)	0.102	0.316	0.320	0.366	0.659	0.586	1.119	1.926
v_t/v_{sph}	0.32	0.22	0.23	0.31	0.37	0.42	0.34	0.32

[b] d_{eq} is the volume equivalent diameter of a sphere, L is the longest, I the intermediate, and S the shortest dimension of the particle. fl is the particle's flatness and el is its elongation. Ψ is the sphericity, which compares the surface area of a particle to that of sphere $\pi d_{eq}^2/SA$, with SA being the surface area of the particle. The Reynolds number Re is defined as $\rho_a v_t d_{eq}/\nu$, where ρ_a is the density and ν is the kinematic viscosity of the air. N is the number of successful experiments. The measured settling velocity v_t is given as the average over the number of experiments of the corresponding shape and size, with σ_{vt} being the standard deviation. v_{rand}, v_{max}, v_{aver}, and v_{sph} are the modeled velocities with random-, maximum-, and average-orientation-drag, and for volume equivalent spheres, respectively.

3.3 Impact on Atmospheric Transport

200 The good agreement between measured and modeled settling velocities allows for the use of the full Bagheri and Bonadonna (2016, 2019) scheme with maximum-orientation-drag for simulating the gravitational settling of glitters in the atmosphere. For this, the scheme has been implemented into the Lagrangian transport model FLEXPART. Figure 3 shows the atmospheric transport potential of glitters, represented by the annual mean of atmospheric horizontal travel distance and residence time, averaged over all six release points. Figures S6-S7 depict annual mean atmospheric travel distances and residence times for each

205 release point separately. Differences in travel distance and residence time that occur between release points can be attributed
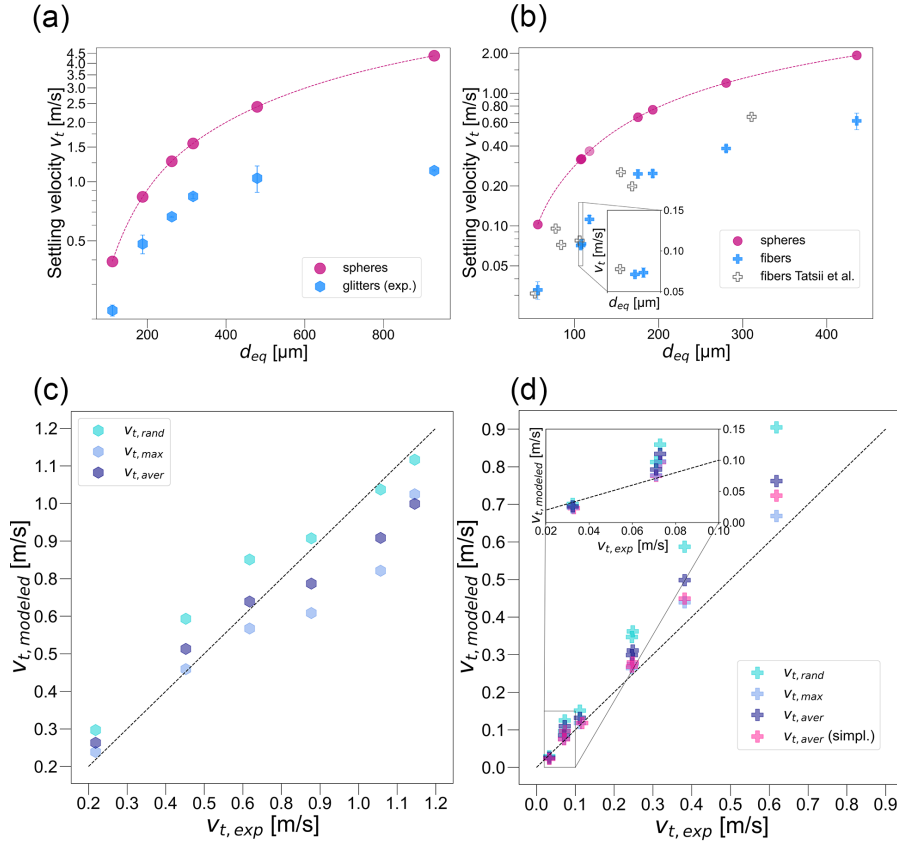
Figure 2. Observed and modeled settling velocities. Measured (blue symbols) settling velocities of glitters (a) and fibers (b) as a function of particle size, expressed as the diameter of a sphere of equivalent volume. Error bars depict the standard deviation. Modeled values of spheres of equivalent volume are shown with pink circles. Blue hexagons (a) and crosses (b) represent experimental results for glitters and fibers, respectively. White crosses in (b) depict previously published experimental results of settling velocities of straight fibers (Tatsii et al., 2024). The inset in (b) shows a closer view of the experimental data on fiber settling velocities. Scatter plot comparing the modeled and measured settling velocities of glitters (c) and fibers (d). Modeled values were calculated with the full model version for random (light blue), maximum-drag (blue) and averaged (dark blue) orientations. In (d), settling velocities of straight fibers modeled with the simplified, average-orientation-drag model (Tatsii et al., 2024) are depicted as well (pink crosses). The inset in (d) shows a closer view of the measured vs. modeled settling velocities of fibers. The dotted line shows the 1:1 relation.

to different meteorological conditions, causing differences, e.g., in vertical transport and, especially, wet deposition. In the following, we concentrate on the results averaged over all release sites.

With increasing equivalent diameter, the particles' mean horizontal atmospheric travel distances resulting from the FLEX-PART simulations decrease (Fig. 3(a)): glitters with nominal diameters of 0.05, 0.1, 0.2, 0.4, 0.6, 1 and 3 mm travel 33.24, 1.52, 210 0.57, 0.48, 0.45, 0.38, and 0.21 km on average, and their volume-equivalent spheres travel 29.47, 1.04, 0.34, 0.22, 0.18, 0.11,
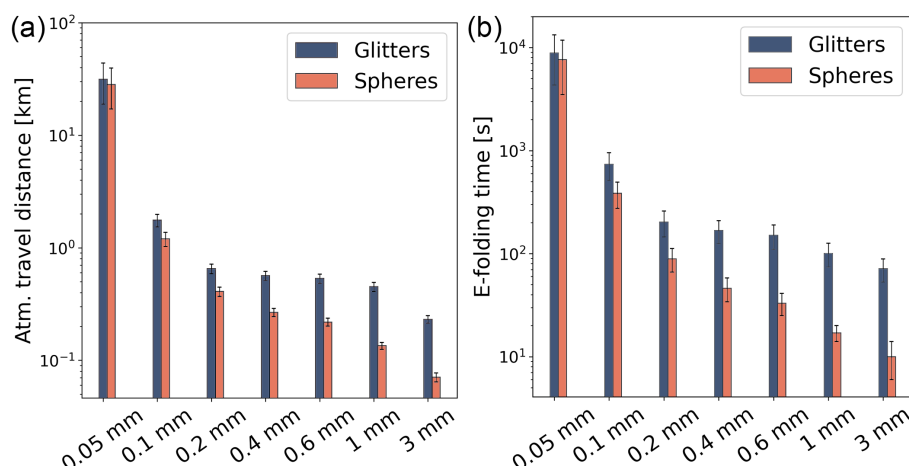
Figure 3. Atmospheric transport potential of glitters and volume-equivalent spheres. Shown are annual mean atmospheric horizontal travel distances (a) and atmospheric residence times (b) of glitters (pink) and spheres (blue). The results are averaged over all release points. Standard deviations are depicted by whiskers.

0.06 km, respectively. The smallest commercially available glitters therefore have the potential to pollute the areas surrounding the cities they are released in, while glitters larger than that are deposited close to their release points and will likely only affect the cities directly. However, resuspension of deposited particles, which is not considered in our simulations, may extend the effective transport distances substantially for all of the studied particles. E-folding times of glitters with nominal diameters of

215   0.05, 0.1, 0.2, 0.4, 0.6, 1 and 3 mm are 146.83, 12.25, 3.36, 2.78, 2.50, 1.67, 1.18 min, respectively, while the residence times of respective volume-equivalent spheres are 127.00, 6.42, 1.48, 0.77, 0.55, 0.28, 0.15 min.

Across all release points, the travel distances of 0.05, 0.1, 0.2, 0.4, 0.6, 1, and 3 mm glitters are 12 ± 5, 48 ± 6, 69 ± 14, 118 ± 11, 147 ± 10, 238 ± 19, and 261 ± 48 % greater than those of volume-equivalent spheres. This can be attributed to the longer atmospheric residence times of nonspherical particles in comparison to spherical ones (Fig. 3(b)). The mean

220   atmospheric residence times of 0.05, 0.1, 0.2, 0.4, 0.6, 1, and 3 mm glitters are 7 ± 14, 90 ± 9, 128 ± 11, 264 ± 41, 346 ± 49, 477 ± 99, 699 ± 213 % longer compared to volume-equivalent spheres. Notice that, similar to the settling velocities, the relative differences between spherical and nonspherical particles for both travel distances and residence times increase with decreasing sphericity.

4   Conclusions

225   The gravitational settling velocities of glitter particles with nominal diameters between 0.1 mm and 3 mm and fibers with lengths between 1.2 and 5 mm were measured in a settling chamber. The observed settling velocities were compared to settling velocities of volume-equivalent spheres and to modeled velocities using the Bagheri and Bonadonna (2016, 2019) shape-correction scheme. We have determined that glitters and fibers settle up to 74 % and 78 % slower compared to volume-

equivalent spheres, respectively. The results are similar to those of Tatsii et al. (2024), who investigated the shape dependency
230   of C_D for 3D-printed, uniform microplastic fibers. They found that settling velocities of fibers are reduced by up to 76 %
compared to volume-equivalent spheres, with highly elongated fibers exhibiting great atmospheric transport potential, capable
of reaching remote locations such as the Arctic, when emitted in populated regions. The good agreement between modeled and
observed settling velocities (average relative differences of 13.2 % for glitters and 12.4 % for fibers) shows that the model is
suitable also for non-ideal, commercially available particles, which often have rough and complex surfaces. This is an important
235   extension of the work of Tatsii et al. (2024) who only used microplastic fibers with perfectly defined shapes.

We use the Lagrangian transport model FLEXPART (Bakels et al., 2024) with an implemented shape correction scheme
(Bagheri and Bonadonna, 2016, 2019) to simulate the atmospheric transport of glitter particles. By that, we have shown that
commercial glitters have relatively large atmospheric transport potential, with the smallest particles traveling up to 33 km.
Our simulation results also demonstrate that microplastic glitters are transported substantially farther than volume-equivalent
240   spheres in the atmosphere: the atmospheric transport distances of microplastic glitters are up to 3.5 times greater than those of
volume-equivalent spheres. This is a result of the longer atmospheric residence times of glitters, with e-folding times up to 7.4
times longer compared to spheres. These results indicate that glitter, when released into the air, may be transported on urban and
regional scales. The same also holds true for microplastic fibers, as shown by Tatsii et al. (2024). This is particularly relevant
for glitter released during parades or carnivals in cities, since airborne glitters may be deposited in soils and water bodies in and
245   outside of the city, including also agricultural fields or conservation areas. Similarly, fibers released, for example from clothes,
could easily be transported beyond the urban area. Especially for the smaller glitters and fibers, the atmosphere therefore
constitutes an important transport medium, which is problematic since these particles are associated with the greatest harm for
organisms and soils (Medyńska-Juraszek and Jadhav, 2022; Provenza et al., 2022). Furthermore, microplastic particles under
weathering processes such as UV radiation, oxidation, or abrasion can degradate and be fragmented (Andrady, 2011), which
250   will increase their transport potential. Resuspension from the ground would further enhance this, with particles potentially
grasshopping several times before being incorporated into the soil matrix or a water body, which may - at least temporarily -
halt the atmospheric transport.

Microplastic films or disks of higher aspect ratios and smaller sizes than considered here might even have larger atmospheric
transport potential, constituting a possible field of further research. Overall, our results enhance the understanding of the shape-
255   dependent settling behavior of airborne microplastics and can be used to constrain atmospheric transport models by accounting
for such complex shapes as hexagonal disks and highly elongated fibers. The size and shape of the glitter particles used in this
work are comparable to other aerosols, exhibiting disk-like shapes, such as plate crystals, mineral dust, pollen, or spores. This
similarity extends the relevance of our work to these other types of particles.

Data availability. The data underlying the study will be made available on Zenodo upon acceptance.

Author contributions. Conceptualization and research design: A.S., G.B., D.T., and A.R.; preparation of the experiments: A.R., T.B., and
G.B.; experiments: A.R. and T.B.; postprocessing of the experimental data: G.B.; analysis of the experimental data: A.R., T.B., and G.B.;
FLEXPART modelling: A.R., D.T., A.S.; analysis of the model results: A.R., D.T., A.S.; visualization: A.R; interpretation of the results:
A.R., D.T., A.S., T.B., G.B; writing - original draft: A.R.; writing - review and editing: A.R., D.T., A.S., T.B., G.B.; supervision: D.T., A.S.,
T.B., and G.B.

Competing interests. The authors declare no competing financial interests.

Acknowledgements. The authors thank Alfredo Soldati, Giuseppe Carlo Alp Caridi, and Vlad Giurgiu from the Institute of Fluid Dynamics
and Heat Transfer, TU Wien, for supplying the fibers and Alexander Bismarck and Qixiang Jiang from the Department of Materials Chemistry, University of Vienna, for providing the pycnometer for the density measurements of the glitter particles. This work was supported by
the University of Vienna's research platform PLENTY - Plastics in the Environment and Society. We would like to thank the Max Planck
Society and the MPI-DS for their support. The Scientific colour map lipari (Crameri, 2018) is used in this study to prevent visual distortion
of the data and exclusion of readers with colour-vision deficiencies (Crameri, 2020).

References

Abbasi, S., Keshavarzi, B., Moore, F., Delshab, H., Soltani, N., and Sorooshian, A.: Investigation of microrubbers, microplastics and heavy metals in street dust: a study in Bushehr city, Iran, Environ. Earth Sci., 76, 1–19, https://doi.org/10.1007/s12665-017-7137-0, 2017.

275 Abbasi, S., Keshavarzi, B., Moore, F., Turner, A., Kelly, F. J., Dominguez, A. O., and Jaafarzadeh, N.: Distribution and potential health impacts of microplastics and microrubbers in air and street dusts from Asaluyeh County, Iran, Environ. Pollut., 244, 153–164, https://doi.org/10.1016/j.envpol.2018.10.039, 2019.

Abessa, D. M. d. S., Albanit, L. F., Moura, P. H. P. d., Nogueira, V. S., Santana, F. T., Fagundes, K., Ueda, M., Muller, O. P. d. O., and Cesar-Ribeiro, C.: A Glow before Darkness: Toxicity of Glitter Particles to Marine Invertebrates, Toxics, 11, https://doi.org/10.3390/toxics11070617, 2023.

280 Allen, S., Allen, D., Phoenix, V. R., Le Roux, G., Durántez Jiménez, P., Simonneau, A., Binet, S., and Galop, D.: Atmospheric transport and deposition of microplastics in a remote mountain catchment, Nat. Geosci., 12, https://doi.org/10.1038/s41561-019-0335-5, 2020.

Ambrosini, R., Azzoni, R. S., Pittino, F., Diolaiuti, G., Franzetti, A., and Parolini, M.: First evidence of microplastic contamination in the supraglacial debris of an alpine glacier, Environ. Pollut., 253, 297–301, https://doi.org/10.1016/j.envpol.2019.07.005, 2019.

285 Andrady, A. L.: Microplastics in the marine environment, Mar. Pollut. Bull., 62, 1596–1605, https://doi.org/10.1016/j.marpolbul.2011.05.030, 2011.

Auta, H., Emenike, C., and Fauziah, S.: Distribution and importance of microplastics in the marine environment: A review of the sources, fate, effects, and potential solutions, Environ. Int., 102, 165–176, https://doi.org/10.1016/j.envint.2017.02.013, 2017.

Bagheri, G. and Bonadonna, C.: On the drag of freely falling non-spherical particles, Powder Technol., 301, 526–544, 290 https://doi.org/10.1016/j.powtec.2016.06.015, 2016.

Bagheri, G. and Bonadonna, C.: Erratum to "On the drag of freely falling non-spherical particles" [Powder Technology 301 (2016) 526–544, DOI: 10.1016/j.powtec.2016.06.015], Powder Technol., 349, 108, https://doi.org/10.1016/j.powtec.2018.12.040, 2019.

Bakels, L., Tatsii, D., Tipka, A., Thompson, R., Dütsch, M., Blaschek, M., Seibert, P., Baier, K., Bucci, S., Cassiani, M., Eckhardt, S., Groot Zwaaftink, C., Henne, S., Kaufmann, P., Lechner, V., Maurer, C., Mulder, M. D., Pisso, I., Plach, A., Subrama-295 nian, R., Vojta, M., and Stohl, A.: FLEXPART version 11: Improved accuracy, efficiency, and flexibility, EGUsphere, 2024, 1–50, https://doi.org/10.5194/egusphere-2024-1713, 2024.

Ballent, A., Corcoran, P. L., Madden, O., Helm, P. A., and Longstaffe, F. J.: Sources and sinks of microplastics in Canadian Lake Ontario nearshore, tributary and beach sediments, Mar. Pollut. Bull., 110, 383–395, https://doi.org/10.1016/j.marpolbul.2016.06.037, 2016.

Bergmann, M., Mützel, S., Primpke, S., Tekman, M. B., Trachsel, J., and Gerdts, G.: White and wonderful? Microplastics prevail in snow 300 from the Alps to the Arctic, Sci. Adv, 5, eaax1157, https://doi.org/10.1126/sciadv.aax1157, 2019.

Bhowmick, T., Seesing, J., Gustavsson, K., Guettler, J., Wang, Y., Pumir, A., Mehlig, B., and Bagheri, G.: Inertia Induces Strong Orientation Fluctuations of Nonspherical Atmospheric Particles, Phys. Rev. Lett., 132, 034 101, https://doi.org/10.1103/PhysRevLett.132.034101, 2024a.

Bhowmick, T., Wang, Y., Latt, J., and Bagheri, G.: Twist, turn and encounter: the trajectories of small atmospheric particles unravelled, 305 https://doi.org/10.48550/arXiv.2408.11487, 2024b.

Blackledge, R. D. and Jones Jr., E. L.: All that Glitters Is Gold!, chap. 1, pp. 1–32, John Wiley & Sons, Ltd, ISBN 9780470166932, https://doi.org/10.1002/9780470166932.ch1, 2007.

Brahney, J., Hallerud, M., Heim, E., Hahnenberger, M., and Sukumaran, S.: Plastic rain in protected areas of the United States, Science, 368, 1257–1260, https://doi.org/10.1126/science.aaz5819, 2020.

310 Cabrera, M., Valencia, B. G., Lucas-Solis, O., Calero, J. L., Maisincho, L., Conicelli, B., Massaine Moulatlet, G., and Capparelli, M. V.: A new method for microplastic sampling and isolation in mountain glaciers: A case study of one antisana glacier, Ecuadorian Andes, CSCEE, 2, 100 051, https://doi.org/10.1016/j.cscee.2020.100051, 2020.

Cai, L., Wang, J., Peng, J., Tan, Z., Zhan, Z., Tan, X., and Chen, Q.: Characteristic of microplastics in the atmospheric fallout from Dongguan city, China: preliminary research and first evidence, ESPR, 24, 24 928–24 935, https://doi.org/10.1007/s11356-017-0116-x, 2017.

315 Chen, P.-H., Droguet, B. E., Lam, I, Green, D. S., Vignolini, S., Gu, Z., De Silva, S., and Reichman, S. M.: Assessing the ecotoxicological effects of novel cellulose nanocrystalline glitter compared to conventional polyethylene terephthalate glitter: Toxicity to springtails (Folsomia candida), Chemosphere, 366, 143 315, https://doi.org/10.1016/j.chemosphere.2024.143315, 2024.

Clift, R. and Gauvin, W. H.: Motion of entrained particles in gas streams, CJCE, 49, 439–448, https://doi.org/10.1002/cjce.5450490403, 1971.

320 Coyle, R., Service, M., Witte, U., Hardiman, G., and McKinley, J.: Modeling Microplastic Transport in the Marine Environment: Testing Empirical Models of Particle Terminal Sinking Velocity for Irregularly Shaped Particles, ACS ES&T Water, 3, 984–995, https://doi.org/10.1021/acsestwater.2c00466, 2023.

Crameri, F.: Scientific colour maps, Zenodo, http://doi.org/10.5281/zenodo.1243862, 2018.

Crameri, F.: The misuse of colour in science communication, Nat. Commun., https://doi.org/10.1038/s41467-020-19160-7, 2020.

325 Das Pramanik, D., Lei, S., Kay, P., and Goycoolea, F. M.: Investigating on the toxicity and bio-magnification potential of synthetic glitters on Artemia salina, Mar. Pollut. Bull., 190, 114 828, https://doi.org/10.1016/j.marpolbul.2023.114828, 2023.

Dehghani, S., Moore, F., and Akhbarizadeh, R.: Microplastic pollution in deposited urban dust, Tehran metropolis, Iran, ESPR, https://doi.org/10.1007/s11356-017-9674-1, 2017.

Dris, R., Gasperi, J., Rocher, V., Saad, M., Renault, N., and Tassin, B.: Microplastic contamination in an urban area: a case study in Greater 330 Paris, Environ. Chem., 12, 592–599, 2015.

Dris, R., Gasperi, J., Saad, M., Mirande, C., and Tassin, B.: Synthetic fibers in atmospheric fallout: A source of microplastics in the environment?, Environ. Pollut., 104, 290–293, https://doi.org/10.1016/j.marpolbul.2016.01.006, 2016.

Dąbrowska, A.: Soil microplastics – current research trends and challenges: preliminary results of the earthworm Eisenia fetida impact on glitters, AHR, 25, 141–150, https://doi.org/10.2478/ahr-2022-0018, 2022.

335 Gray, A. D. and Weinstein, J. E.: Size- and shape-dependent effects of microplastic particles on adult daggerblade grass shrimp (Palaemonetes pugio), ET&C, 36, 3074–3080, https://doi.org/https://doi.org/10.1002/etc.3881, 2017.

Green, D. S., Jefferson, M., Boots, B., and Stone, L.: All that glitters is litter? Ecological impacts of conventional versus biodegradable glitter in a freshwater habitat, J. Hazard. Mater., 402, 124 070, https://doi.org/10.1016/j.jhazmat.2020.124070, 2021.

Harley-Nyang, D., Memon, F. A., Jones, N., and Galloway, T.: Investigation and analysis of microplastics in sewage 340 sludge and biosolids: A case study from one wastewater treatment works in the UK, Sci. Total Environ., 823, 153 735, https://doi.org/10.1016/j.scitotenv.2022.153735, 2022.

Hartmann, N., Hüffer, T., Thompson, R., Hasselöv, M., Verschoor, A., Daugaard, A., Rist, S., Karlsson, T., Brennholt, N., Cole, M., Herrling, M., Hess, M., Ivleva, N., Lusher, A., and Wagner, M.: Are We Speaking the Same Language? Recommendations for a Definition and Categorization Framework for Plastic Debris., Environ. Sci. Technol., 53, 1039–1047, https://doi.org/10.1021/acs.est.8b05297, 2019.

345   Hersbach, H., Bell, B., Berrisford, P., Hirahara, S., Horányi, A., Muñoz-Sabater, J., ..., and Thépaut, J. N.: The ERA5 global reanalysis, Q. J. R. Meteorol. Soc., 146, 1999–2049, https://doi.org/10.1002/qj.3803, 2020.

Kim, D., Kim, H., and An, Y.-J.: Effects of synthetic and natural microfibers on Daphnia magna–Are they dependent on microfiber type?, Aquat. Toxicol., 240, 105 968, https://doi.org/https://doi.org/10.1016/j.aquatox.2021.105968, 2021.

Kwak, J. I., Liu, H., Wang, D., Lee, Y. H., Lee, J.-S., and An, Y.-J.: Critical review of environmental impacts of microfibers in different
350   environmental matrices, CPBC, 251, 109 196, https://doi.org/https://doi.org/10.1016/j.cbpc.2021.109196, 2022.

Liu, K., Wang, X., Fang, T., Xu, P., Zhu, L., and Li, D.: Source and potential risk assessment of suspended atmospheric microplastics in Shanghai, Sci. Total Environ., 675, 462–471, https://doi.org/10.1016/j.scitotenv.2019.04.110, 2019a.

Liu, K., Wu, T., Wang, X., Song, Z., Zong, C., Wei, N., and Li, D.: Consistent Transport of Terrestrial Microplastics to the Ocean through Atmosphere, Environ. Sci. Technol., 53, 10 612–10 619, https://doi.org/10.1021/acs.est.9b03427, pMID: 31408609, 2019b.

355   Luana Lume Yoshida, I. B. J. and da Cunha-Santino, M. B.: Interference of glitter with the photosynthetic rates of a submerged macrophyte, Egeria densa, N. Z. J. Bot., 0, 1–14, https://doi.org/10.1080/0028825X.2023.2276284, 2023.

Lusher, A. L., Hurley, R., Vogelsang, C., Nizzetto, L., and Olsen, M.: Mapping microplastics in sludge, NIVA, https://niva.brage.unit.no/ niva-xmlui/handle/11250/2493527, 2017.

Machado, M. J., Dextro, R. B., Cruz, R. B., Cotta, S. R., and Fiore, M. F.: Response of two cyanobacterial strains to non-biodegradable glitter
360   particles, Aquat. Toxicol., 260, 106 590, https://doi.org/10.1016/j.aquatox.2023.106590, 2023.

Market Research Intellect: Glitter Powder Market Size By Product, By Application, By Geography, Competitive Landscape And Forecast, https://www.marketresearchintellect.com/product/global-glitter-powder-market/, 2025.

Medyńska-Juraszek, A. and Jadhav, B.: Influence of Different Microplastic Forms on pH and Mobility of Cu2+ and Pb2+ in Soil, Molecules, 27, https://doi.org/10.3390/molecules27051744, 2022.

365   Newsom, R. and Bruce, C.: The dynamics of fibrous aerosols in a quiescent atmosphere, Phys. Fluids, 6, 521–530, 1994.

Nithin, A., Sundaramanickam, A., and Sathish, M.: Seasonal distribution of microplastics in the surface water and sediments of the Vellar estuary, Parangipettai, southeast coast of India, Mar. Pollut. Bull., 174, 113 248, https://doi.org/10.1016/j.marpolbul.2021.113248, 2022.

Petersen, F. and Hubbart, J. A.: The occurrence and transport of microplastics: The state of the science, Sci. Total Environ., 758, 143 936, https://doi.org/10.1016/j.scitotenv.2020.143936, 2021.

370   Pisso, I., Sollum, E., Grythe, H., Kristiansen, N. I., Cassiani, M., Eckhardt, S., Arnold, D., Morton, D., Thompson, R. L., Groot Zwaaftink, C. D., Evangeliou, N., Sodemann, H., Haimberger, L., Henne, S., Brunner, D., Burkhart, J. F., Fouilloux, A., Brioude, J., Philipp, A., Seibert, P., and Stohl, A.: The Lagrangian particle dispersion model FLEXPART version 10.4, GMD, 12, 4955–4997, https://doi.org/10.5194/gmd-12-4955-2019, 2019.

Prata, J. C.: Airborne microplastics: Consequences to human health?, Environ. Pollut., 234, 115–126,
375   https://doi.org/10.1016/j.envpol.2017.11.043, 2018.

Preston, C. A., McKenna Neuman, C. L., and Aherne, J.: Effects of Shape and Size on Microplastic Atmospheric Settling Velocity, Environ. Sci. Technol., 57, 11 937–11 947, https://doi.org/10.1021/acs.est.3c03671, pMID: 37523322, 2023.

Provenza, F., Anselmi, S., Specchiulli, A., Piccardo, M., Barceló, D., Prearo, M., Pastorino, P., and Renzi, M.: Sparkling plastic: Effects of exposure to glitter on the Mediterranean mussel Mytilus galloprovincialis, Environ. Toxicol. and Pharmacol., 96, 103 994,
380   https://doi.org/https://doi.org/10.1016/j.etap.2022.103994, 2022.

Qi, G. Q., Nathan, G. J., and Kelso, R. M.: PTV measurement of drag coefficient of fibrous particles with large aspect ratio, Powder Technol., 229, 261–269, https://doi.org/10.1016/j.powtec.2012.06.049, 2012.

Raju, S., Carbery, M., Kuttykattil, A., Senthirajah, K., Lundmark, A., Rogers, Z., SCB, S., Evans, G., and Palanisami, T.: Improved methodology to determine the fate and transport of microplastics in a secondary wastewater treatment plant, Water Res., 173, 115 549, https://doi.org/10.1016/j.watres.2020.115549, 2020.

385 Romanó de Orte, M., Clowez, S., and Caldeira, K.: Response of bleached and symbiotic sea anemones to plastic microfiber exposure, Environ. Pollut., 249, 512–517, https://doi.org/https://doi.org/10.1016/j.envpol.2019.02.100, 2019.

Saxby, J., Beckett, F., Cashman, K., Rust, A., and Tennant, E.: The impact of particle shape on fall velocity: Implications for volcanic ash dispersion modelling, J. Volcanol. and Geotherm. Res., 362, 32–48, https://doi.org/10.1016/j.jvolgeores.2018.08.006, 2018.

390 Song, Y., Cao, C., Qiu, R., Hu, J., Liu, M., Lu, S., Shi, H., Raley-Susman, K. M., and He, D.: Uptake and adverse effects of polyethylene terephthalate microplastics fibers on terrestrial snails (Achatina fulica) after soil exposure, Environ. Pollut., 250, 447–455, https://doi.org/https://doi.org/10.1016/j.envpol.2019.04.066, 2019.

Tagg, A. S. and Ivar do Sul, J. A.: Is this your glitter? An overlooked but potentially environmentally-valuable microplastic, Mar. Pollut. Bull., 146, 50–53, https://doi.org/10.1016/j.marpolbul.2019.05.068, 2019.

395 Tatsii, D., Bucci, S., Bhowmick, T., Guettler, J., Bakels, L., Bagheri, G., and Stohl, A.: Shape Matters: Long-Range Transport of Microplastic Fibers in the Atmosphere, Environ. Sci. Technol., 58, 671–682, https://doi.org/10.1021/acs.est.3c08209, 2024.

Tinklenberg, A., Guala, M., and Coletti, F.: Thin disks falling in air, J. Fluid Mech., 962, A3, https://doi.org/10.1017/jfm.2023.209, 2023.

Tinklenberg, A., Guala, M., and Coletti, F.: Turbulence effect on disk settling dynamics, J. Fluid Mech., 992, A4, https://doi.org/10.1017/jfm.2024.534, 2024.

400 Willmarth, W. W., Hawk, N. E., and Harvey, R. L.: Steady and Unsteady Motions and Wakes of Freely Falling Disks, Phys. Fluids, 7, 197–208, https://doi.org/10.1063/1.1711133, 1964.

Yurtsever, M.: Glitters as a Source of Primary Microplastics: An Approach to Environmental Responsibility and Ethics, J. Agric. Environ. Ethics, 32, 459 – 478, https://doi.org/10.1007/s10806-019-09785-0, 2019a.

Yurtsever, M.: Tiny, shiny, and colorful microplastics: Are regular glitters a significant source of microplastics?, Mar. Pollut. Bull., 146,
405 678–682, https://doi.org/10.1016/j.marpolbul.2019.07.009, 2019b.

Zanini, M. L. d. O., Fonseca, L. M., Piecha, C. R., Corrêa, C. d. P. L., Dode, L. B., Zavareze, E. d. R., and Diaz, P. S.: A Review of Conventional and Environmentally Sustainable Glitter, Environ. Qual. Manag., 34, e22 322, https://doi.org/10.1002/tqem.22322, 2024.

Zhang, Y., Kang, S., Allen, S., Allen, D., Gao, T., and Sillanpää, M.: Atmospheric microplastics: A review on current status and perspectives, Earth-Sci. Rev., 203, 103 118, https://doi.org/10.1016/j.earscirev.2020.103118, 2020.

410 Zhou, Q., Tian, C., and Luo, Y.: Various forms and deposition fluxes of microplastics identified in the coastal urban atmosphere, Chin. Sci. Bulletin, 62, 3902–3909, https://doi.org/10.1360/N972017-00956, 2017.